KOHN, V. G. (1979*b*). *Kristallografiya*, **24**, 712-719.
KOZMIK, V. D. & MIKHAILYUK, I. P. (1978*a*). *Ukr. Fiz. Zh. (Ukr. Ed.)* **23**, 1570-1571.
KOZMIK, V. D. & MIKHAILYUK, I. P. (1978*b*). *Pis'ma Zh. Eksp. Teor. Fiz.* **28**, 673-674.
LEVONYAN, L. V. (1981). *Pis'ma Zh. Tech. Fiz.* **7**, 269-272.
PINSKER, Z. G. (1978). *Dynamical Scattering of X-rays in Crystals.* Heidelberg, New York: Springer-Verlag.
SUVOROV, E. V. & POLOVINKINA, V. I. (1974). *Pis'ma Zh. Eksp. Teor. Fiz.* **20**, 328-329.

Acta Cryst. (1986). A**42**, 435-441

The Intercomparison of Bragg X-ray Reflections from a Small Single Crystal – Zero-Wavelength-Dispersion Profile Measurement

BY A. MCL. MATHIESON* AND A. W. STEVENSON

Division of Chemical Physics, CSIRO, PO Box 160, *Clayton, Victoria, Australia* 3168

(*Received* 10 *December* 1985; *accepted* 21 *February* 1986)

Abstract

In conventional one-dimensional profile measurement procedures, either by diffractometry ('counter' profile) or by photography ('film' profile), intercomparison of Bragg reflections from a small single crystal, c, in a given experiment is rendered difficult, or impossible, by their wide variation in size with θ_c. Using synthetic $I(\Delta\omega, \Delta 2\theta)$ distributions, obtained by convolution of four components, the mosaic spread of the specimen crystal, μ, the emissivity distribution of the source, σ, its wavelength distribution, λ, and the detector aperture, δ, analysis shows how the 'counter' and 'film' profiles change with scan mode. In particular, it is shown that the 'film' profile obtained using an $\omega/2\theta$ ($s=2$) scan mode does not involve wavelength dispersion, so that the profile distribution can yield information about μ for each reflection and therefore about small differences in mosaic spread (and hence reflectivity) between reflections. Possible means of obtaining this profile using film or counter procedures are outlined.

Introduction

The intrinsic two-dimensional nature of the $\Delta\omega, \Delta 2\theta$ measurement procedure (Mathieson, 1982) and the detailed information which, with adequate resolution, it can yield, establishes it as a powerful means of investigating Bragg X-ray reflections from small single crystals. The 2D distribution can allow one to diagnose and estimate the individual linear distributions associated with the major components of the experiment, such as the mosaic-spread distribution of the specimen crystal, μ, the emissivity distribution of the X-ray source, σ, and its wavelength distribution, λ. With a minor experimental modification (Mathieson & Stevenson, 1984), the main components can be reduced to two, μ and λ, which can then be defined more precisely (Mathieson & Stevenson, 1985) so that variation of mosaic spread μ (*alias* reflectivity distribution, r - see Mathieson, 1984*a*) across a 60 μm crystal could be estimated (Mathieson & Stevenson, 1986).

Because the data are recorded in two dimensions, the $\Delta\omega, \Delta 2\theta$ measurement procedure is necessarily slower than one-dimensional procedures. It is, therefore, likely that, for reasons of convenience and speed, essentially one-dimensional procedures will continue to be used for routine data-collection tasks.

There is, however, no reason to assume, merely because of long-established usage, that the 1D procedures which are in current use necessarily supply either the best information or the available information in the best form. In this paper, we re-examine, from the $\Delta\omega, \Delta 2\theta$ viewpoint, the possibilities of 1D measurement - (*a*) to determine if there is any variant which would improve the quality of the 1D measurement and (*b*) to indicate possible advantageous ways of using position-sensitive detectors (p.s.d.'s) for 1D measurement when such detectors become available with sufficient spatial (angular) resolution.

Current one-dimensional procedures

In the currently conventional 1D measurement of Bragg X-ray reflections from a small single crystal, c, two main procedures are used. One involves a counter diffractometer using a wide aperture in front of the detector, the other uses photographic film. In attempting to compare reflections within a given experiment by either procedure, a basic difficulty results from the wide variation in the size of reflections. *Inter alia*, this feature complicates intrinsic problems in measurement, such as the distinction of what is peak and what is background, correction for thermal

* Present address: Department of Chemistry, La Trobe University, Bundoora, Victoria, Australia 3083.

0108-7673/86/060435-07$01.50

diffuse scattering, *etc.* Indeed, as a result of this overriding effect, it is almost impossible to seek for and detect, by direct experimental comparison with these procedures, the components responsible for finer differences between reflections. If all reflections from a given crystal could be reduced to a more comparative scale, then one would be in an improved position to identify and quantify those shades of difference between them which relate to changes in specimen-specific properties with orientation, such as anisotropic mosaic spread.

The component which stretches out Bragg reflections systematically with increase in θ_c is, of course, the wavelength distribution of the source and it is this which renders any direct comparison between reflections almost impossible when using conventional one-dimensional procedures. In theory, one can visualize the possibility of applying corrections for the wavelength distribution, for example, by deconvolution, to remove that λ component and reduce the observed intensity distribution to a non-dispersive condition. However, Bragg reflections are generally complex in their internal structure, being generated by the convolution of several major and minor components, see, for example, Alexander & Smith (1962), who treat the matter in one dimension. Deconvolution of a one-dimensional distribution into individual components in such circumstances may be tricky, if not impossible, and the mathematical operations may not lead to unique or physically realistic results.

Examination from the $\Delta\omega, \Delta 2\theta$ viewpoint

Let us therefore start *ab initio* and consider, in general terms, what is measured in the conventional 1D procedures.* To examine the situation in a systematic manner, we will utilize the $\Delta\omega, \Delta 2\theta$ viewpoint and, to exemplify the effect of θ_c, take (*a*) a lower-angle reflection with $\theta_c = 10°$ and (*b*) a higher-angle reflection with $\theta_c = 60°$. This corresponds to a wavelength dispersion ratio of approximately 1 : 10.

To illustrate the various aspects of this examination and avoid the possibly confusing influence of random errors (noise) which would go with the use of purely experimental data, we make use of synthetic distributions, *cf.* Schoenborn (1983) on neutron diffraction reflections from protein crystals. These distributions are generated by convolution, in $\Delta\omega, \Delta 2\theta$ space, of the various linear functions for μ, σ, λ and δ, the last referring to the contribution from the detector aperture. Guided by values derived from earlier studies, *e.g.* Mathieson (1982, 1984*b*), the following parameter values were chosen; (i) for the source, σ, a trapezoidal distribution of base 0·075° and full width at half height 0·06° (in terms of $\Delta\omega$); (ii) for the wavelength distribution λ, two Lorentzian peaks of relative height 2·0 : 1·0* and widths at half height of 0·460 and 0·635 mÅ, respectively (see Hoyt, 1932; Parratt, 1936), for a wavelength of 1·5418 Å and with the two components separated by 0·0038 Å; (iii) for the crystal, regarded as vanishingly small in size, a mosaic spread, μ, represented by a Gaussian with full width at half height of 0·06° $\Delta\omega$. A minor component for the detector aperture, δ, represented by a square wave of base 0·02° $\Delta 2\theta$, was also included for completeness. Convoluting these four components together, we obtain for the lower- and higher-Bragg-angle reflections 2D distributions at steps of 0·01° in both $\Delta\omega$ and $\Delta 2\theta$. These are shown in contour form in Figs. 1(*a*) and (*b*), respectively. They have been calculated for the ω (or $s = 0$) scan mode (for terminology, see Mathieson, 1983*a*). We use the superscript (s) to identify an item with a particular scan mode. The distributions are calculated over the whole rectangular area $P^{(0)}Q^{(0)}R^{(0)}S^{(0)}$ associated with the conventional wide-aperture width ($\Delta 2\theta_2 - \Delta 2\theta_1$) and the specimen-crystal scan width ($\Delta\omega_2 - \Delta\omega_1$). Note that this area changes with scan mode. The eight-sided figure *ABCDEFGH*, corresponding to the truncation limits for the three main components, μ, σ, λ, and the minor component δ, does not change in area with change in scan mode and represents a proper comparative estimate of integrated intensity (Mathieson, 1982).

The counter diffractometer procedure which uses a wide aperture in front of the detector corresponds to the integration of the signal, $I(\Delta\omega, \Delta 2\theta^{(0)})$, across the aperture for each setting of $\Delta\omega$ and therefore yields the one-dimensional 'counter' profile

$$I(\Delta\omega) = \int_{\Delta 2\theta_1^{(0)}}^{\Delta 2\theta_2^{(0)}} I(\Delta\omega, \Delta 2\theta^{(0)}) \mathrm{d}(\Delta 2\theta^{(0)}). \quad (1)$$

The resultant 'counter' profile curves, derived from integrating across the rectangular area $P^{(0)}Q^{(0)}R^{(0)}S^{(0)}$, are shown on the right of Figs. 1(*a*) and (*b*).

The photographic procedure corresponds to integration of the signal, $I(\Delta\omega, \Delta 2\theta^{(0)})$, for each point $\Delta 2\theta^{(0)}$, as the specimen crystal steps along $\Delta\omega$, and therefore yields the one-dimensional 'film' profile curve†

$$I(\Delta 2\theta^{(0)}) = \int_{\Delta\omega_1}^{\Delta\omega_2} I(\Delta\omega, \Delta 2\theta^{(0)}) \, \mathrm{d}(\Delta\omega). \quad (2)$$

The resultant 'film' profile curves, derived from

* We refer here to the experimental situation without a monochromator. Mathieson (1985) has considered the inclusion of a monochromator in the basic experimental set-up, in terms of $\Delta\omega, \Delta 2\theta$ space.

* For demonstration purposes, the ratio used is of the appropriate order, although in actual cases, it can be significantly different from 2·0.

† It should be pointed out that, in reality, the minor component δ has no meaning for the photographic procedure, and therefore should not be included when deriving the 'film' profile. Its inclusion, however, makes little or no difference here.

integrating down the rectangular area $P^{(0)}Q^{(0)}R^{(0)}S^{(0)}$, are shown below Figs. 1(a) and (b). [In each case, the conventional final integrated intensity (including background) is obtained by integration over $\Delta\omega$ or $\Delta 2\theta^{(0)}$ respectively.]

For the $\omega(s=0)$ scan mode, the wavelength dispersion effect occurs in both the 'counter' and 'film' profiles. This is evidenced clearly by the higher-angle reflections; see the profiles on the right of and below Fig. 1(b), the angular dispersion in the latter being twice that in the former.

We now consider the situation when the detector is displaced synchronously with the displacement of the specimen crystal, in a 1:1 relationship [ω/θ (or $s=1$) scan mode], Fig. 2, and in a 2:1 relationship [$\omega/2\theta$ (or $s=2$) scan mode], Fig. 3. The $I(\Delta\omega, \Delta 2\theta^{(s)})$ distributions change appropriately. In each figure, the rectangular areas corresponding to the wide-aperture procedure, $P^{(1)}Q^{(1)}R^{(1)}S^{(1)}$ and $P^{(2)}Q^{(2)}R^{(2)}S^{(2)}$, respectively, are shown, as well as the eight-sided figure *ABCDEFGH*, the area of which is invariant with respect to s and corresponds to the 2D truncated area for the proper estimation of integrated intensity. As far as the 1D procedures are concerned, the resultant projected distributions for the 'counter' profile and the 'film' profile (which both relate to the rectangular areas) are shown on the right and below the respective 2D distribution.

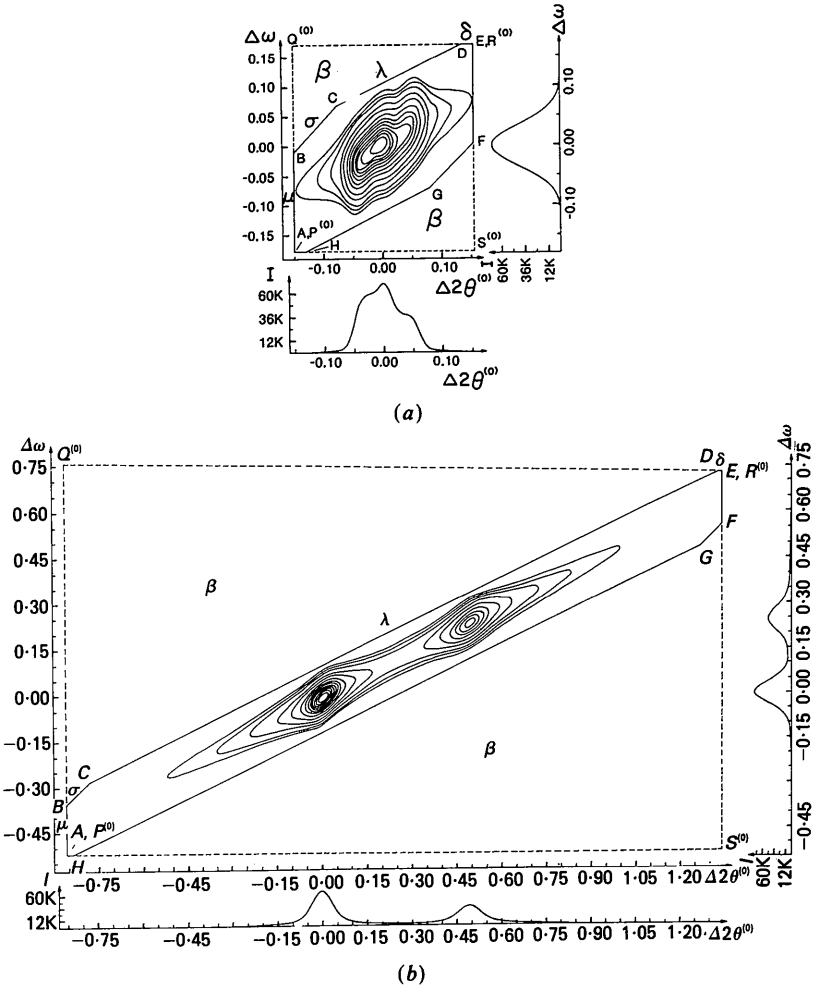

Fig. 1. Synthetic distributions, $I(\Delta\omega, \Delta 2\theta^{(0)})$, in the ω-scan mode, for (a) a low-angle reflection, $\theta_c = 10°$, and (b) a higher-angle reflection, $\theta_c = 60°$. The components, in angular terms, are (i) the mosaic-spread distribution, μ, a Gaussian of FWHH = 0·06°$\Delta\omega$, (ii) the source distribution, σ, a trapezoid of base 0·075° and FWHH 0·06° (in terms of $\Delta\omega$) and (iii) the wavelength distribution, λ, two Lorentzian distributions, corresponding to an average wavelength of 1·5418 Å, of peak height 1·0 and FWHH = 0·460 mÅ, and the other of peak height 0·5 and FWHH = 0·635 mÅ, separated by $\Delta\lambda = 0{\cdot}0038$ Å. A minor component, the detector aperture, δ, is also included and represented by a square wave of base 0·02° $\Delta 2\theta$. $P^{(0)}Q^{(0)}R^{(0)}S^{(0)}$ represents the area encompassed by the 1D procedure, with $P^{(0)}S^{(0)}$ representing the wide aperture and $P^{(0)}Q^{(0)}$ the angular range of the specimen crystal scan. *ABCDEFGH* represents the area encompassed by exactly truncated limits of the components μ, σ, λ, δ; limits which apply for all reflections. The 'counter' profile derived by projection along the $\Delta 2\theta^{(0)}$ axis within the limits of $P^{(0)}Q^{(0)}R^{(0)}S^{(0)}$ is shown on the right while the 'film' profile, derived by projection along the $\Delta\omega$ axis within the same area $P^{(0)}Q^{(0)}R^{(0)}S^{(0)}$, is shown below the 2D distribution. For reasons of practicability and clarity of presentation, the scale of Figs. 1(a), 2(a) and 3(a) is twice that of Figs. 1(b), 2(b) and 3(b).

All three 'counter' profile curves, on the right of Figs. 1(*b*), 2(*b*) and 3(*b*), due to integration parallel to $\Delta 2\theta$, involve the wavelength dispersion to very much the same extent. There will be, both in principle and in practice, small differences between these three profiles because, with the wide aperture, the different scan modes give rise to different areas outside the eight-sided figure, *i.e.* the areas designated β in Figs. 1, 2 and 3, and so collect different background signal.

In the case, however, of projection along $\Delta\omega$, *i.e.* the 'film' profile, the contribution from the wavelength dispersion changes markedly with change in scan mode, being, in this group, largest for the ω-scan mode, reduced to half for the ω/θ scan mode and to zero for the $\omega/2\theta$ scan mode; see the profiles below Figs. 1(*b*), 2(*b*) and 3(*b*) and compare with those below Figs. 1(*a*), 2(*a*) and 3(*a*). [Denne (1977) has, as part of his description and assessment of a technique for using the ω/θ scan for X-ray monochromatization, shown photographs which correspond to 'film' profiles for that scan mode.]

The last case is therefore of some interest in respect of 1D procedures. Its possibility does not appear to have been exploited previously although an indication of its capability was given by Mathieson (1983*b*). This case shows that if one can devise a means, while operating in the $\omega/2\theta$ scan mode, either of recording in 'photographic space' or of integrating along $\Delta\omega$, then one can derive a 1D profile which effectively eliminates the contribution of the wavelength distribution, leaving only the main components μ_{hkl} and σ, which are relatively invariant, convoluted together, *i.e.* $\mu_{hkl} * \sigma$, with minor components. Under such circumstances, the profile curves for *all reflections* will then be essentially $\mu_{hkl} * \sigma$, and therefore more readily compared so that differences associated with $\mu(\equiv r)$ should be detectable.

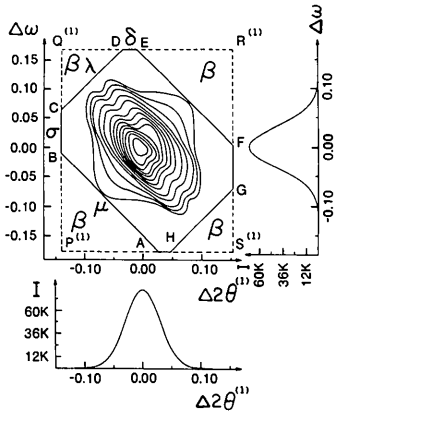

(*a*)

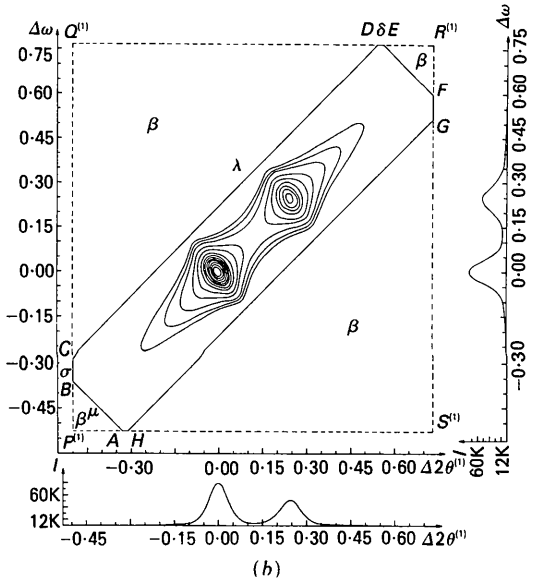

(*b*)

Fig. 2. The synthetic distribution, presented here in the ω/θ scan mode, *i.e.* $I(\Delta\omega, \Delta 2\theta^{(1)})$, for (*a*) the low-angle reflection and (*b*) the higher-angle reflection, with the resultant 'counter' and 'film' profiles on the right and below, respectively.

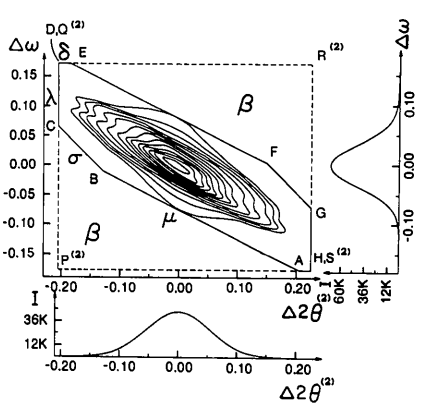

(*a*)

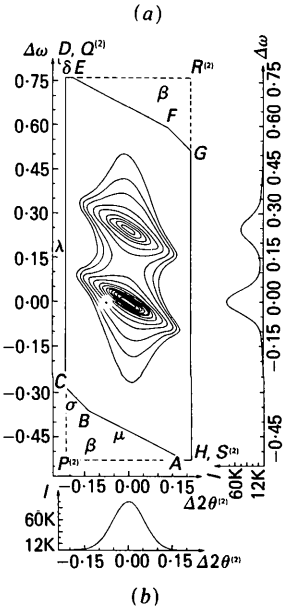

(*b*)

Fig. 3. The synthetic distribution, presented here in the $\omega/2\theta$ scan mode, *i.e.* $I(\Delta\omega, \Delta 2\theta^{(2)})$, for (*a*) the low-angle reflection and (*b*) the higher-angle reflection, with the resultant 'counter' and 'film' profiles on the right and below, respectively.

Zero-wavelength-dispersion profile measurement

Measurement of Bragg reflection profiles with the wavelength contribution zero can be realized for both photographic and counter methods.

1. *Photographic method*

This is feasible with an appropriate elaboration of the Weissenberg method. Fig. 4 illustrates the scheme. The necessary modification involves the film holder being rotated while it makes its usual traverse parallel to the rotation axis of the crystal. The layer-line screen restricts the recordable reflections to the zero layer (say) and they pass through to record on the film. While the crystal rotates in a right-handed sense at the rate $\dot{\omega}$, the film holder should rotate in the same direction at $2\dot{\omega}$ and simultaneously traverse parallel to the rotation axis. This helical movement of the film holder requires that there is a helical slot in the film holder which gives access for the incident beam and its collimator. A simple demonstration of the effect of this type of angular motion on an individual reflection (without the linear traverse component) can be given by placing a small film on the front of the detector of a diffractometer and making an exposure while operating in the $\omega/2\theta$ scan mode. The comparative result for a lower- and a higher-angle reflection is shown in Figs. 5(*a*)(iii) and (*b*)(iii), revealing their essential similarity. For completeness (and comparison with Figs. 1, 2 and 3, the film profiles for $s = 0$, 1 and 2 are shown in Fig. 5. Strangely enough, although from the viewpoint presented in this paper it appears an obvious test to make, we do not know of its having been carried out previously with this purpose in mind.*

It will be appreciated that, with the modified Weissenberg method, there will be a small amount of λ dispersion due to the linear traverse component of the film holder but this lies at right angles to the dispersion associated with the mosaic spread convoluted with the source size, $\mu * \sigma$. To minimize this, the linear traverse of the film holder should be made as small as is feasible to avoid merging of reflections on adjacent rows. For example, if a 180° rotation of the crystal corresponds to a 90 mm traverse of the film holder then a 1° scan in ω would lead to an extension of the spot by 0·5 mm. Since this extension is at right angles to the $\mu * \sigma$ distribution, it does not modify the essential form of that distribution.

Protein crystal data are often collected with a series of films (see Arndt & Wonacott, 1977), each film involving only a limited angular displacement of the

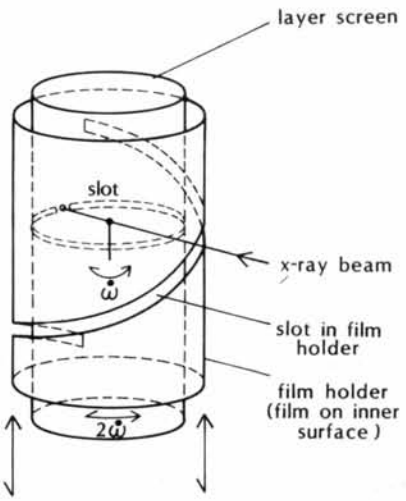

Fig. 4. Elaboration of the Weissenberg method to allow the film to rotate about the specimen crystal axis at twice the rate of angular rotation of the specimen crystal. The layer-line screens allow only the zero layer (say) to pass to the film. A helical slot in the film and film holder allows the incident beam and its collimator through.

* One author, AMcLM, is convinced of having seen an early reference by K. Lonsdale to an effective ω/θ scan of a single reflection by mounting a film holder arm on the crystal axle of a Weissenberg camera but has been unable to trace this work. A similar set-up was used by Wooster (1945) to derive a topograph of a small crystal.

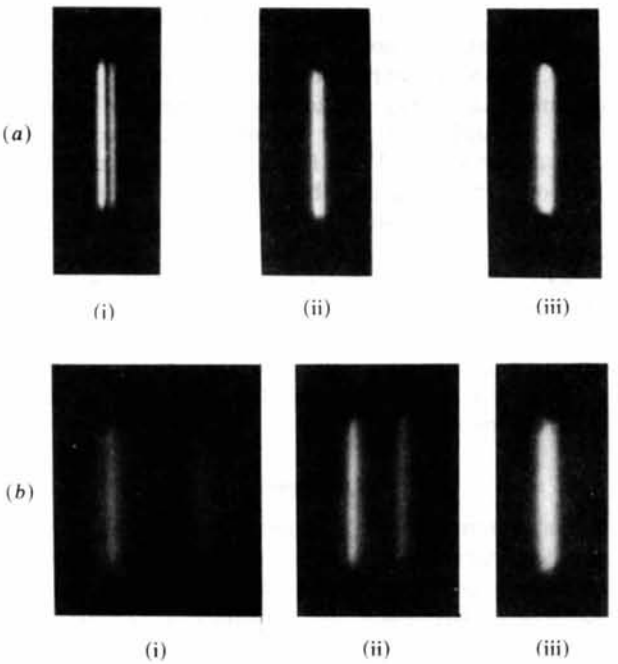

Fig. 5. Photographs ('film' profiles) of Bragg reflections taken on a diffractometer by placing a film on the front of the detector. They are recorded for (*a*) a lower θ_c and (*b*) a higher θ_c value (actually 12·6 and 60·7°, respectively) for the scan modes (i) $s = 0$, (ii) $s = 1$ and (iii) $s = 2$. The specimen used was a small (~0·1 mm) imperfect single crystal of cubic K_2SnCl_6. The reflections used were both orders of the $01\bar{1}$, namely the $02\bar{2}$ and $08\bar{8}$, so that only ω and 2θ had to be changed, *i.e.* the mosaic spread is essentially unchanged. The incident radiation was unfiltered Cu $K\alpha$ from a line focus (see Mathieson & Stevenson, 1984*a*,*b*).

specimen crystal. With this arrangement, it would be relatively simple, mechanically, to rotate the film holder at an angular rate twice that of the crystal and hence obtain the array of reflections on each film with zero wavelength dispersion at right angles to the rotation axis. For reflections on upper layers the amount of elongation increases with n, the layer-line number. This procedure may have a minor practical advantage in giving an indication of reflection truncation due to incomplete angular scan (see Arndt & Wonacott, 1977, p. 8).

2. *Counter method*

As is evident from the discussion above, it is not feasible to realize this procedure on a diffractometer using a scintillation counter and a conventional wide aperture. It can be achieved however if one uses a narrow aperture in front of the detector to record a single value of $I(\Delta 2\theta)$ and tracks with the detector assembly in the $\omega/2\theta$ scan mode - the so-called 'slice scan' (Mathieson, 1983*b*). This is necessarily a relatively slow process.

To render it more expeditious, one is required to use a linear position-sensitive detector so that one is collecting the complete series of $I(\Delta 2\theta)$ readings for any given $\Delta\omega$ simultaneously, rather than reading one at a time. It is preferable under those circumstances that the real (and not merely apparent) resolution of the p.s.d. should correspond to or be better than the minimum $\Delta 2\theta$ step of the detector arm, *i.e.* that the p.s.d. should have real resolution of *ca* 0·1 mm, equivalent to *ca* 0·01°. So far as synthetic distributions are concerned, the distribution across pixels due to the intrinsic diffusion of each quantum could be modelled, if necessary, by a Gaussian for δ.

Naturally, use of a p.s.d. would allow fully 2D operation but, if only the zero-wavelength-dispersion 1D profile was sought, then this would simply mean storing the integrals over $\Delta\omega$ (for each pixel) or preferably across the appropriate section of the eight-sided figure *ABCDEFGH*.

Discussion

Some comments are warranted concerning the 1D profiles derived with the different scan modes (excluding from consideration the effects of multiple scattering, discussed by Mathieson, 1984*a*). As observed above, the 'counter' profiles for s = 0, 1 and 2 scan modes are essentially the same apart from different contributions from the area $P^{(s)}Q^{(s)}R^{(s)}S^{(s)} - ABCDEFGH$ for the different s values. The situation is different with respect to the 'film' profiles. For $s = 0$, the profile corresponds to the convolution of σ and λ and the detector aperture, δ, with zero contribution from μ. For $s = 1$, the profile corresponds to the convolution of μ, λ and δ, with zero contribution from σ. For $s = 2$, the profile corresponds to the convolution of μ, σ and δ, with zero contribution from λ. These observations are summarized in Table 1; '(2)' adjacent to a component in the table indicates the situations in respect of the 'film' profile where the components are 'stretched out' to twice their $\Delta\omega$ range.

Table 1. *Change of component contribution with scan mode*

	$s=0$	$s=1$	$s=2$
'Counter' profile	$\mu * \sigma * \lambda$	$\mu * \sigma * \lambda$	$\mu * \sigma * \lambda$
'Film' profile	$\sigma * (2)\lambda * \delta$	$\mu * \lambda * \delta$	$(2)\mu * \sigma * \delta$

It should be noted that the observations summarized in Table 1 refer to a profile derived by projection. Thus, in the case of the 'film' profile, this requires an angular scan of the specimen crystal sufficient to ensure complete integration. A film record taken at only one setting of $\Delta\omega$ would yield only a section of the 2D $\Delta\omega$, $\Delta 2\theta$ distribution and not a projection. It would therefore provide information which, while involving all three (four including δ) components to some extent, would be incomplete and therefore liable to misinterpretation. To illustrate that the scan mode can influence critically the interpretation of the resultant 'film' profile, we refer to an example recorded by James (1948), namely the results of Ehrenberg & Mark (1927). This involved a small 'perfect' crystal of diamond and stationary-film records (*i.e.* $s = 0$) made at a distance from the specimen crystal of 10 m for the reflections 111 and 333 and 6 m for 555. The angular ranges for 111, 333 and 555, instead of decreasing as expected from theoretical considerations, increased as 5·5, 13·2 and 39″, respectively. Ehrenberg & Mark (1927) ascribed this trend mainly to wavelength dispersion and the present examination provides confirmation of this interpretation, see Fig. 5(i). From the viewpoint developed here and the test results shown in Fig. 5(iii), it would be of interest to re-examine this (or a similar) experiment on a 'perfect' crystal using an $s = 2$ scan of the film.

With the possibility of determining the reflectivity curve for each reflection from an 'imperfect' crystal, one can visualize the derivation of a single universal curve of correction for extinction *versus* reflectivity point by point for the particular crystal specimen founded on an essentially experimental basis (see, for example, Schneider, 1977) rather than the general practice of correction based on theoretical modelling. The present set-up does not require specialized facilities, unlike the case for γ-rays.

Although the present study is directed at the measurement of Bragg reflections from small single crystals (and, of course, selected-area diffraction from larger plate-shaped crystals) for the purpose of deriving reflectivity curves and integrated intensity, it also has bearing on aspects of the measurement of X-ray spectra (and absorption edges). If dealing with a

spectrometer with a single dispersing crystal with $\mu \simeq 0$ (*i.e.* a 'perfect' crystal) and a source of very small dimension in the plane of diffraction then a 'film' profile with $s = 0$ has twice the angular dispersion of the 'counter' profile (see Fig. 1*b*). This suggests the possibility of increasing the numerical dispersion of the 'film' profile by using a non-standard 'inverse' scan mode with $s = -1, -2$, *etc.* to increase the effective dispersion relative to the 'counter' profile by 3, 4, *etc.*

We are most grateful to Dr S. L. Mair for allowing us to use her K_2SnCl_6 specimen. One of us (AWS) acknowledges the financial support of a CSIRO Postdoctoral Award.

References

ALEXANDER, L. E. & SMITH, G. S. (1962). *Acta Cryst.* **15**, 983-1004.
ARNDT, U. W. & WONACOTT, A. J. (1977). *The Rotation Method in Crystallography.* Amsterdam: North-Holland.
DENNE, W. A. (1977). *Acta Cryst.* A**33**, 987-992.
EHRENBERG, W. & MARK, H. (1927). *Z. Phys.* **42**, 807-822.
HOYT, A. (1932). *Phys. Rev.* **40**, 477-483.
JAMES, R. W. (1948). *The Optical Principles of the Diffraction of X-rays.* London: Bell.
MATHIESON, A. McL. (1982). *Acta Cryst.* A**38**, 378-382.
MATHIESON, A. McL. (1983*a*). *J. Appl. Cryst.* **16**, 257-258.
MATHIESON, A. McL. (1983*b*). *Acta Cryst.* A**39**, 79-83.
MATHIESON, A. McL. (1984*a*). *Acta Cryst.* A**40**, 355-363.
MATHIESON, A. McL. (1984*b*). *Aust. J. Phys.* **37**, 55-61.
MATHIESON, A. McL. (1985). *Acta Cryst.* A**41**, 309-316.
MATHIESON, A. McL. & STEVENSON, A. W. (1984). *Aust. J. Phys.* **37**, 657-665.
MATHIESON, A. McL. & STEVENSON, A. W. (1985). *Acta Cryst.* A**41**, 290-296.
MATHIESON, A. McL. & STEVENSON, A. W. (1986). *Acta Cryst.* A**42**, 223-230.
PARRATT, L. G. (1936). *Phys. Rev.* **50**, 1-15.
SCHNEIDER, J. R. (1977). *Acta Cryst.* A**33**, 235-243.
SCHOENBORN, B. P. (1983). *Acta Cryst.* A**39**, 315-321.
WOOSTER, N. (1945). *J. Sci. Instrum.* **22**, 132.

Acta Cryst. (1986). A**42**, 441-449

On the Theory of Six-Beam X-ray Spherical-Wave Diffraction

BY V. G. KOHN

I. V. Kurchatov Institute of Atomic Energy, 123182, *Moscow, USSR*

AND A. H. TONEYAN

Department of Physics, Erevan State University, Erevan, USSR

(*Received* 20 *October* 1983; *accepted* 27 *March* 1986)

Abstract

A general formula is obtained for the intensity distribution in the film behind a single crystal in the case of spherical-wave X-ray multiple diffraction. The theory takes into account the phase shift of the waves not only inside the crystal but also in the vacuum before and after the crystal along the wave path source-crystal-film of length L. The topographic images are calculated in the case of (220/242/044/$\bar{2}$44/$\bar{2}$02) six-beam diffraction of Cu $K\alpha$ radiation in a germanium crystal of thickness 0·2 mm for different values of L. The enhancement of the anomalous transmission effect is weakly displayed on the topographs because of strong scattering of the radiation inside the crystal. The intensity distribution depends on L. The possibility is shown of focusing X-rays to a considerable extent.

1. Introduction

In recent years the scheme shown in Fig. 1 has been widely used for experimental investigations of X-ray multiple diffraction in single crystals. The divergent radiation of the microbeam X-ray tube falls directly on a crystal in the form of a plate with thickness t. The intensity of diffracted beams is determined by the darkening of the film placed behind the crystal [see, for example, the papers by Balter, Fildman & Post (1971), Huang & Post (1973), Kshevetskii & Mihailyuk (1976), Mihailyuk, Kozmik & Kshevetskii (1977)]. To enlarge the section of the topographs corresponding to multiple-beam angles of incidence

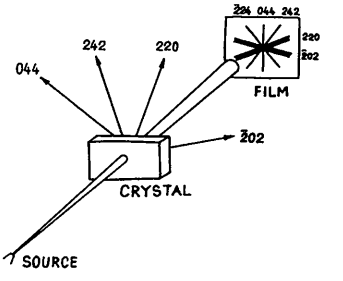

Fig. 1. Scheme of the experiment for investigating X-ray multiple diffraction.

0108-7673/86/060441-09$01.50